Cell-Counting Algorithm for Automatic Identification of Fluorescent Cell Images

Jae Hyuk Lee[1], Sung Han Rhim[2], Young Woong Sohn[1], Pyeong Soo Park[1], Yoon Kim[1], Myoung Shin Kim[1], Young Hun Kim[1], Cham Han Lee[1], Jeong Mi Moon[1], Byung Hee Jeon[1], Jong Kil Lee[3]

[1] *CytoGen, Inc., Seoul, Korea*
[2] *Department of Mechanical Engineering, Dankook University, Yong-in, Kyonggi-do, Korea*
[3] *Department of Mechanical Engineering, Korea Polytechnic University, Siheung, Kyonggi-do, Korea*

Corresponding author: Sung Han Rhim

CytoGen, Inc.

52 Chungmin-ro, Songpa-gu

Seoul 138–961, Republic of Korea

Email: shrhim@cytogenlab.com

Tel: +82-2-6925-1070

Fax: +82-2-6925-1071

Abbreviations used: CLC, Cancer cell Lline Control; WBC, White Blood Cell; CK, CytoKeratin; DAPI, 4’6-diamidino-2-phenylindole; PBS, Phosphate Buffer Saline; BSA, Bovine Serum Albumin; CCD, Charge Coupled Device;

Running title: An automated cell identification and counting

Abstract

To overcome this, imaging processing techniques have been applied to continue the development of the automatic cell-counting method in order to count fluorescence-stained cancer cells in the field of cytology automation. However, because the fluorescent intensities of fluorescence-stained cells are outputted differently, it is difficult to count cells automatically. Thus, the standardization of fluorescence intensities, which were outputted differently from cells, was established and a cell-counting algorithm that can perform automatic cell counting through the standardization was developed in the present study.

In the present study, immunofluorescence staining was conducted with six types of cancer cell-line controls using DAPI, CK, and CD45 and analyzed through the developed fluorescence-based optical system in order to verify the accuracy and reliability of the cell-counting algorithm developed in the present study.

Each CLC showed 95% accuracy for each CLC using the cell-counting algorithm, and the SD was ±0.027. The present study also proved that the correlation coefficient of automatic counting was 0.991 through regression analysis. The accuracy and reliability of the cell-counting algorithm used in the present paper were proven through verification tests using each of the CLCs, and the algorithm is expected to be applied to various fluorescence staining-based analyses.

Keyword: automated cell counting, cell morphology, Analysis, cell counting algorithm

Introduction

It is critical to ensure the counting of cancer cells clinically is accurate. This is because the number of cancer cells in blood can be a measure for predicting the state of patients [1]. The accurate detection and analysis of cancer cells for accurate cancer cell counting contribute to cancer diagnosis through clear understanding on cancer development, clinical treatment efforts for cancer patients, medical development, and mechanical research [2–3]. However, the number of cancer cells detected in patients is small and varies depending on the state of the patient, which is why accurate counting by humans is regarded as highly difficult. Even if cell counting can be performed accurately by humans, the results can vary even with the same sample due to reading variability.

In order to count cancer cells without errors, standardized and automated processes will be integrated into a single flow. In the field of cytology automation, research on the processes that isolate cancer cells involving fluorescence-stained followed by performing an automatic counting method has been performed continuously [4–7]. Immunofluorescence staining is a process that is conducted in priority to identify cancer cells. It is proposed because it is difficult to count cancer cells automatically through imaging analysis if the cells are observed using general microscopes, as cancer cells are seen as transparent water droplets. Fluorescence staining helps identify cancer cells using fluorescence-based optical microscopes. The counting method is performed with images produced from fluorescence-based optical microscopes. The outputted images support the analysis of the morphology and intensity of cells through the imaging process technique-applied algorithm, and automatic counting can be conducted based on the analysis [8–9].

Cancer cells are identified as follows: Cancer cells extracted via purification assays are verified through a typical cancer cell marker (CK), leukocyte marker (CD45), and nuclear staining (DAPI) in order to distinguish cancer cells from leukocytes. Here, cancer cells are identified with DAPI (+) positive, CK (+) positive, and CD45 (-) negative, and white blood cells (WBCs) are identified with DAPI (+) positive, CK (-) negative, and CD45 (+) positive. The identified cancer cells are all listed. However, because fluorescent intensities of fluorescence-stained cells are outputted differently, it is difficult to count cancer cells automatically. Thus, the standardization of fluorescence

intensities, which were outputted differently from cells, was established, and a cell-counting algorithm that can perform automatic cell counting through the standardization was developed in the present study. The cell-counting algorithm is a system that performs counting automatically through image processing based on morphology characteristics, such as size, area, area intensity, and circularity [10–15].

In the present study, tests were conducted using six types of cancer cell-line controls (CLCs) (DU145, H358, H460, H2228, LNCaP, and PC9) in order to verify the accuracy and reliability of the cell-counting algorithm developed by our company.

Materials and Methods

Sample Preparation

The samples fabricated in the present study were divided into A-Type, B-Type, C-Type, and D-Type. The CLCs used in the test were H358, H460, H2228, LNCaP, Du145, and PC9. A-Type was made by mixing about 100 WBCs with the CLCs. The mixed cells were fixed with 4% paraformaldehyde for 5 min, air-dried, and attached to a glass slide. For A-Type, each CLC had five samples, so a total of 30 A-Type samples were made. A-Type is a sample for comparing the counting results of the automatic mode with those using the manual mode when the cell-counting algorithm was applied to the CLCs. B-Type was made by mixing about 100 WBCs with the following approximate numbers of PC9 cells: 10, 50, 100, and 300. Three glass slides to which about 10 PC9 cells were attached, three glass slides to which about 50 PC9 cells were attached, three glass slides to which about 100 PC9 cells were attached, and finally one glass slide to which about 300 PC9 cells were attached were fabricated. B-Type is a sample for verifying the linear correlation coefficient of the cell-counting algorithm and proving its accuracy. For C-Type, only one sample was fabricated by attaching about 1,000 WBCs. C-Type is a sample for setting the cut-off range with regard to WBCs. D-Type was fabricated by attaching about 1,000 CLCs only in contrast with C-Type. For D-Type, each CLC had a single sample, so a total of six D-Type samples were made. D-Type is a sample for setting the cut-off range with regard to each CLC.

Immunofluorescent staining

Cells on slides were permeabilized with 0.2% Triton-X 100 in phosphate buffer saline (PBS) for 10 min. Cells were then blocked with 1% bovine serum albumin (BSA) in PBS for 30 min and incubated with primary antibodies followed by secondary antibodies. The primary antibodies were mouse anti-pan CK (Sigma) and rabbit anti-CD45 (Cell Signaling Technology). The secondary antibody was goat anti-rabbit Alexa 647 (Invitrogen) and goat anti-mouse Alexa 488 (Invitrogen). The slides were mounted with Fluoroshield with DAPI (ImmunoBioScience). The staining protocol was applied to all samples equivalently.

Imaging detection

It is necessary to maintain fluorescence reflectance constantly in order to shoot the fluorescence samples and analyze the images. The fluorescence intensity stained in cells weakens over time [16]. Inconsistent fluorescence reflectance makes counting difficult because it is correlated to the fluorescence intensity of each cell. Thus, it is necessary to have a rule that can maintain and analyze the cell fluorescence rate in the glass slide constantly. The samples were stored in a cartridge that can block the light after completing fluorescence staining in order to maintain the fluorescence rate for each cell and shoot in sequence. Light was blocked from the samples prior to shooting.

A cell image analyzer device, which was developed at our company, was used to shoot the glass slide. The lenses mounted on the device had magnitudes of 4x, 10x, 20x, and 40x, and a 10x magnitude lens was used in the present study. The charge-coupled device (CCD) (Infinity 3-3UR) was the mono type, and each image had 1936x1456 pixels. The lighting (SOLA SM II) was a white light type whose wavelength ranged from 380nm–680nm. For the filter, UV2A was used to shoot DAPI, and for CK, FITC was used, and for CD45, Cy5 was used (the fluorescence filters were from Nikon). The images shot via each of the filters were used to count the CLCs. To set up the CCD for shooting the CLCs, only exposure time and gain value were applied. In order to shoot DAPI, CK, and CD45 in the same conditions and environment, the exposure time and gain value were set to 400 ms and 5x, respectively. The intensity of the lighting was set to 15% for

DAPI, 5% for CK, and 60% for CD45.

It was necessary to have focusing essentially to shoot cell images. Since the level of focusing with the 10x lens was 8.5 micrometers, precise control was required. If a cell was shot out of the 8.5 micrometer range, its boundary was blurred, making counting difficult. If blurred cell images are counted, data, such as area, diameter, and fluorescence intensity data, are not reliable. In the present study, all samples were focused to be inside the 8.5-micrometer range, thereby enabling the extraction of clear images of all ranges for the accurate extraction of cell shapes.

The stained cells in the glass slide were distributed in an 8-mm-diameter circle range. The range of 8 mm was the index set to be applied to the cell image analyzer. The cell image analyzer can shoot a total area in the 8-mm-diameter circle automatically. The total number of images that were shot in the 8-mm-diameter circle area was 120, and they were stitched to make a single image to be applied to the counting algorithm. Each of the three filters produced a stitched image, so a total of three images were obtained. Fig. 1A shows the procedure of image extraction from the samples sequentially.

Cell Counting Algorithm

The cell-counting algorithm is a system that performs counting automatically through image processing based on morphology characteristics, such as size, area, fluorescence intensity, and circularity. The cell-counting algorithm identifies cells and counts them automatically. Fig. 1B shows a flow chart for the cell-counting algorithm. First, a DAPI image is opened and thresholding is performed. Thresholding refers to the conversion of a 24-bit color image into a 1-bit image after binarization. In a 1-bit image, the fluorescence intensity is outputted to 0 or 1 only from a single pixel. Binarization is a widely used technique that can simplify complex images, such as 24-bit images, into 0 or 1 in order to analyze and process them. Using the area, diameter, and other cell data from the binarized images, first and second filtering are performed to detect cells. The first filtering is conducted to eliminate image noise. Image noise is related to the background of the image. Noise in the binarized image is represented as 1 in the pixel, which is distributed widely over the background in the image. Normally, a general white image can be seen clearly even with a low exposure time in the CCD, whereas

fluorescent images cannot show a fluorescence sample if the exposure time is low. Thus, a fluorescence sample has to be observed with a long exposure time in fluorescent images, and noise occurs due to a long exposure time. Since noise influences cell identification, the filtering of noise is needed. The second filtering is to eliminate foreign matters. Foreign matters are expressed with various types in contrast with noise. For example, the following cases are recognized as foreign matters if an image shape is larger than that of a cell, if a diameter of a shape is larger than that of a cell, or if the shape is not a cell. In order to perform the second filtering, the cut-off range of the area and diameter of the cell is set and inputted into the algorithm. The unit of the cut-off diameter and area of the cell is pixels, and a pixel is 1.2 micrometers in size. After the first and second filtering, the image coordinates are implemented through the detected DAPI. The cells detected in the DAPI image are also located in the same spots in CK and CD45 images. Thus, the coordinates of cells extracted from the DAPI image are synchronized with the coordinates of CK and CD45. A rectangular range as large as the cell size is drawn through the synchronized coordinates of each cell. The mean value of fluorescence intensity is calculated and stored for every rectangular range through the coordinates of DAPI, CK, and CD45. Fluorescence intensity refers to the color intensity of each pixel, which is expressed as a number through which a cell can be identified. The stored data, such as the area, diameter, and fluorescence intensity of cells, are used to count the cells automatically.

The analyzed cell data are expressed as a graph. The graph is used to verify the automatic counting result. The X and Y axes in the graph can represent the cell data selectively. The selectively represented data can be the cell number, area, diameter, or fluorescence intensity. The X-axis in the graph of Fig. 2A represents the mean value of fluorescence intensity in the CK image, and the Y-axis represents the mean value of the fluorescence intensity in the CD45 image. The images extracted through the graph represent the cell types that are counted in the present study.

Fig. 2B shows CLCs that are identified through the cell-counting algorithm. The cell identification method for the CK and CD45 images other than DAPI is distinguished by (-) negative and (+) positive and identified via the cut-off range of fluorescence intensity. The CK and CD45 image of each CLC has a different cut-off range of fluorescence intensity distinguished by (-) negative and (+) positive [17]. The difference in the (+)

positive cut-off range in CK and CD45 from CLC to CLC is due to the characteristics of CLCs and the light wavelength intensity that is reflected to the CLCs through the filters. This is because every DAPI, CK, and CD45 has a different range of excitation and the lighting also has different exposure strength in every region of the wavelength. The reaction level to fluorescence is also different from CLC to CLC, which can be a variable. To set the (+) positive cut-off range as mentioned above, it is necessary to study the identification of each CLC beforehand. C-Type and D-type are the samples used to set the (+) positive cut-off range of the CLCs and WBCs.

Results and Discussion

Set-up of (+) positive cut-off range

Fig. 1B shows two parts of the cut-off range in the algorithm: one is the area and diameter, and the other is the intensity. Thus, a preliminary test was conducted to set the cut-off range of each CLC and WBC prior to executing cell counting. First, fluorescence-stained C-Type and D-Type samples with only CLCs and WBCs were fabricated and images were extracted through the cell image analyzer. By applying the cell-counting algorithm to the extracted images, the area, diameter, and intensity of the CLCs and WBCs were analyzed. Figs. 3 and 4 show graphs of the results.

Fig. 3A shows the mean diameter of each cell. The unit of the Y-axis is pixels, and each pixel is 1.2 micrometers. The mean diameter was a value extracted from the DAPI images. The results were as follows: 4.9 pixels for WBCs, 7.6 pixels for PC9, 8.2 pixels for LNCaP, 7.0 pixels for H2228, 6.9 pixels for H460, 7.0 pixels for H358, and 6.5 pixels for DU145. The standard deviation (SD) of the error bar was calculated by 95% confidence intervals [18]. The SDs of WBCs, PC9, LNCaP, H2228, H460, H358, and DU145 were ±1.5, ±2.1, ±2.3, ±1.8, ±1.8, ±1.8, and ±1.9, respectively. Fig. 3B shows the mean area of each cell. The unit of the Y-axis is pixels, and the area was calculated. The mean area was a value extracted from the DAPI images. The results were as follows: 32.0 pixels for WBCs, 76.3 pixels for PC9, 87.9 pixels for LNCaP, 65.0 pixels for H2228, 62.7 pixels for H460, 63.7 pixels for H358, and 56.5 pixels for DU145. The SD of the error bar was also calculated 95% confidence intervals. The SDs of WBCs,

PC9, LNCaP, H2228, H460, H358, and DU145 were ±25.0, ±47.1, ±51.4, ±37.3, ±33.2, ±35.5, and ±35.7, respectively. Based on the above data, the cut-off range for the diameter and area was set. To count all cells, the upper and lower limits in the cut-off range were set to the maximum and minimum values in the error bar among all the cells. The upper limits of the cut-off range for diameter and area were 10.5 pixels and 139.3 pixels, which were the maximum values of LNCaP, and the lower limits were 3.4 pixels and 7.0 pixels, which were the minimum values of WBCs.

Fig. 4 shows the intensity value of each cell. The X-axis represents the number of cells distributed over each sample, and the Y-axis represents the cell intensity (0–225) of the CK and CD45 images. P1 refers to the upper limit in each graph, mean refers to the mean value, and P2 refers to the lower limit. The upper and lower limits are the maximum and minimum values in the error bar through SD. The lower limit of the cut-off range of CK was based on the upper limit of WBCs, and the upper limit was based on the upper limit of PC9. This was because the upper limit of WBCs was lower than the lower limit of the CLCs. Similarly, CD45 was also based on WBCs; the upper limit was applied without change, but the mean value was applied for the lower limit. This was because the lower limit of WBCs was applied higher than the upper limit of the CLCs in order to distinguish the CLCs from WBCs. As shown in the CD45 graph, the mean value of WBCs was higher than the upper limit of the CLCs. The finally set intensity cut-off values of the CK image were 7 and 255, which were the limit values of WBCs and PC9, while the intensity cut-off values of CD45 were 64 and 121, which were the upper limit and mean value of WBCs. Since the unit of the intensity cut-off range was pixels, all decimal points were rounded up. If the intensities of cells in CK and CD45 were within this range, the cells were identified as (+) positive in each image. The reason for the same cut-off range between the WBCs and CLCs was to comply with the purpose of the automatic cell counting.

Cell counting

The automatic and manual counting results were similar after applying the set cut-off range to the cell-counting algorithm and manual counting the B-Type samples. B-Type refers to a sample where 10ea, 50ea, 100ea, and 300ea of PC9 were attached to

each glass slide. Fig. 5A shows a graph that compares the counting results between automatic and manual counting. The X-axis represents the number of samples counted manually, while the Y-axis represents the number of samples counted automatically. The two results are represented with a distribution format, and the regression analysis results are shown with a linear trend line. Here, the correlation coefficient was 0.9991, which indicated that the reliability of the cell-counting algorithm according to the number of CLCs was 99.9%.

A-Type samples, which were fabricated in order to verify the accuracy for other CLCs, were also counted. A-Type was a sample made by mixing CLCs and WBCs. A total of five samples were prepared for each CLC. The sample was used for verification to distinguish CLCs from WBCs and count CLCs only accurately. Fig. 5B shows a graph of automatic counting results with percentages based on the manual counting results for each CLC. The X-axis represents each CLC, and the Y-axis represents the manual and automatic mean counting percentages. As shown in the graph, each CLC showed 95% accuracy for each CLC using the cell-counting algorithm, and the SD was ±0.027. The accuracy of the cell-counting algorithm for various types of CLCs was verified through the above results.

Conclusion

The accuracy and reliability of the cell-counting algorithm with regard to the analysis and counting of various CLCs were verified. A difference in the features between CLCs and WBCs was clearly seen by analyzing the mixed CLCs and WBCs. For PC9, H358, and WBC, the intensities of CK and CD45 were clearly distinguished, but LNCaP, H2228, H460, and DU145 were not clearly distinguished. However, this issue was about the re-establishment of the staining rule for each CLC and not within the scope of the present paper. Rather, the present study proved the accuracy of the cell-counting algorithm through the unclearly distinguished intensities, which contributes to the automatic counting field of fluorescent cells positively.

The cell-counting algorithm was analyzed through the setup of the cut-off range, which produced no reproduction error. In contrast, since manual counting is performed by individuals, different errors can be produced even if the same samples are counted. It is

difficult for humans to count 1,000 or more CLCs manually. On the other hand, if counting is performed via devices embedded with the cell-counting algorithm, 10,000 cells can be analyzed and counted within 15 min automatically. The cell-counting algorithm can be applied to not only the cell image analyzer developed by our company, but also any device. The cell-counting algorithm can contribute to the field of cytology automation significantly.

The accuracy and reliability of the cell counting algorithm used in the present paper were proven through verification tests using each of the CLCs, and the algorithm is expected to be applied to various fluorescence staining-based analyses and contribute to accurate cell analysis in the future.

References

[1] C. G. Loukas, G. D. Wilson, B. Vojnovic, A. Linney,_An image analysis-based approach for automated counting of cancer cell nuclei in tissue sections, Cytom. Part A. 55 A (2003) 30–42.

[2] S. Park, R. R. Ang, S. P. Duffy, J. Bazov, K. N. Chi, P. C. Black, and H. Ma, Morphological differences between circulating tumor cells from prostate cancer patients and cultured prostate cancer cells, PLoS One. 9 (2014) e85264.

[3] F. A. Coumans, S. T. Ligthart, and L. W. Terstappen, Interpretation of changes in circulating tumor cell counts, Transl. Oncol. 5 (2012) 486–91.

[4] S. T. Ligthart, F. W. Coumans, G. Attard, A. M. Cassidy, J. S. Bono, L. M. M. Terstappen, Unbiased and Automated Identification of a Circulating Tumour Cell Definition That Associates with Overall Survival, PLoS One. 6 (2011) e27419.

[5] J. Nieva, M. Wendel, and M. Luttgen, High-definition imaging of circulating tumor cells and associated cellular events in non-small cell lung cancer patients: a longitudinal analysis, Phys. Biol. 9 (2012) 016004.

[6] T. M. Scholtens, F. Schreuder, S. T. Ligthart, J. F. Swennenhuis, J. Greve, and L. W. M. M. Terstappen, Automated identification of circulating tumor cells by image cytometry, Cytom. Part A. 81 A (2012) 138–148.

[7] P. Gogoi, S. Sepehri, Y. Zhou, M. A. Gorin, C. Paolillo, E. Capoluongo, K. Gleason, A. Payne, B. Boniface, M. Cristofanilli, T. M. Morgan, P. Fortina, K. J. Pienta, K. Handique. Y. Wang, Development of an Automated and Sensitive Microfluidic Device for Capturing and Characterizing Circulating Tumor Cells (CTCs) from Clinical Blood Samples, PLoS One. 11 (2016) e0147400.

[8] M. Zhao, P. G. Schiro, J. S. Kuo, K. M. Koehler, D. E. Sabath, V. Popov, Q. Feng, D. T. Chiu, An Automated High-Throughput Counting Method for Screening Circulating Tumor Cells in Peripheral Blood, Anal Chem. 85(4) (2013) 2465-2471.

[9] B. K. Al-Khazraji, P. J. Medeiros, N. M. Novielli, D. N. Jackson,_An automated cell-counting algorithm for fluorescently-stained cells in migration assays, Biological Procedures Online. (2011) 13-9.

[10] E. S. Lianidou and A. Markou, Circulating tumor cells in breast cancer: Detection systems, molecular characterization, and future challenges, Clin. Chem. 57 (2011)

1242–1255.
[11] E. H. E. Cho, M. Wendel, M. Luttgen, C. Yoshioka, D. Marrinucci, D. Lazar, E. Schram, J. Nieva, L. Bazhenova, A. Morgan, A. H. Ko, W. M. Korn, A. Kolatkar, K. Bethel, and P. Kuhn, Characterization of circulating tumor cell aggregates identified in patients with epithelial tumors, Phys. 9 (2012) 016001.
[12] M. Wendel, L. Bazhenova, R. Boshuizen, A. Kolatkar, P. Thistlethwaite, K. Bethel, J. Nieva, M. Van Den Heuvel, and P. Kuhn, Fluid biopsy for circulating tumor cell identification in patients with earl and late stage non-small cell lung cancers; a glimpse into lung cancer biology, Phys. Biol. 9 (2012) 016005.
[13] D. Marrinucci, K. Bethel, A. Kolatkar, M. Luttgen, M. Malchiodi, F. Baehring, K. Voigt, D. Lazar, J. Nieva, L. Bazhenova, A. H. Ko, W. M. Korn, E. Schram, M. Coward, X. Yang, T. Metzner, R. Lamy, M. Honnatti, C. Yoshioka, J. Kunken, Y. Petrova, D. Sok, D. Nelson, and P. Kuhn, Fluid biopsy in patients with metastatic prostate, pancreatic, and breast cancers, Phys. Biol. 9 (2012) 016003.
[14] K. G. Phillips, A. Kolatkar, K. J. Rees, R. Rigg, D. Marrinucci, M. Luttgen, K. Bethel, P. Kuhn, and O. J. T. McCarty, Quantification of cellular volume and sub-cellular density fluctuations: comparison of normal peripheral blood cells and circulating tumor cells identified in a breast cancer patient, Front. Oncol. 2 (2012) 1–10.
[15] E. Hye, J. Kil, B. Chul, S. Han, J. Wook, K. Hee, S. Mok, P. Soo, H. Chul, J. Lee, and B. Hee, Enrichment of cancer cells from whole blood using a microfabricated porous filter, Anal. Biochem. 440 (2013) 114–116.
[16] D. P. Hong, G. H. Lee, N. C. Jung, M. G. Jeon, Fast automated yeast cell counting algorithm using bright field and fluorescence microscopic images, Biological Procedures Online. (2013) 15-13.
[17] B. M. Dent, L. F. Ogle, R. L. O'Donnell, N. Hayes, U. Malik, N. J. Curtin, A. V. Boddy, E. R. Plummer, R. J. Edmondson, H. L. Reeves, F. E. B. May, D. Jamieson, High resolution imaging for the detection and characterisation of circulating tumour cells from patients with oesophageal, hepatocellular, thyroid and ovarian cancers, IJC. 138 (2016) 206-216.
[18] D. G. Altman, J. M. Bland, How to obtain the confidence interval from a P value, BMJ. 343 (2011) d2090.

Figure Legends

Figure 1. Sample preparation process and a flow chart of the cell-counting algorithm. (A) Prepared glass slide is mounted on the cell image analyzer system, and images are shot. Focusing is performed by controlling the depth of focus of cells wherever cells are shot, and DAPI, EpCAM, and CD45 images are extracted. (b) A flow chart for the cell-counting algorithm.

Figure 2. Cell-counting program and identified types of cancer cells. (A) The cell-counting algorithm-applied program and identification method. The X-axis in the graph represents the mean value of fluorescence intensity of the CK image, and the Y-axis represents the mean value of fluorescence intensity in the CD45 image. The images extracted through the graph represent cell types that are counted in the present study. (b) CLCs that are identified through the cell-counting algorithm. The cell identification method for CK and CD45 images other than DAPI is distinguished by (-) negative and (+) positive and identified via the cut-off range of fluorescence intensity.

Figure 3. Analysis of area and diameter to set up the cut-off range of cell size. By applying the cell-counting algorithm, the area and diameter of CLCs and WBCs are analyzed. (A) The mean diameter of each cell. The unit of the Y-axis is pixels, and each pixel is 1.2 micrometers long. The mean diameter is a value extracted from DAPI images. (B) The mean area of each cell. The unit of the Y-axis is pixels, and the area is calculated. The mean area is a value extracted from DAPI images.

Figure 4. Analysis of fluorescence intensity to set up the (+) positive cut-off range. The graph expresses the intensity value of each cell. The X-axis represents the number of cells distributed over each sample, and the Y-axis represents the cell intensity (0–225) of the CK and CD45 images. P1 refers to the upper limit in each graph, mean refers to the mean value, and P2 refers to the lower limit. The upper and lower limits are the maximum and minimum values in the error bar through SD.

Figure 5. Counting results after applying the cell-counting algorithm. (A) The graph

compares the counting results between automatic and manual counting. The X-axis represents the number of samples counted manually, while the Y-axis represents the number of samples counting automatically. The linear trend line is the regression analysis results of two results via the distribution chart. (B) A graph of automatic counting results with percentages based on the manual counting results for each CLC. The X-axis represents each CLC, and the Y-axis represents the manual and automatic mean counting percentages.

Figure. 1

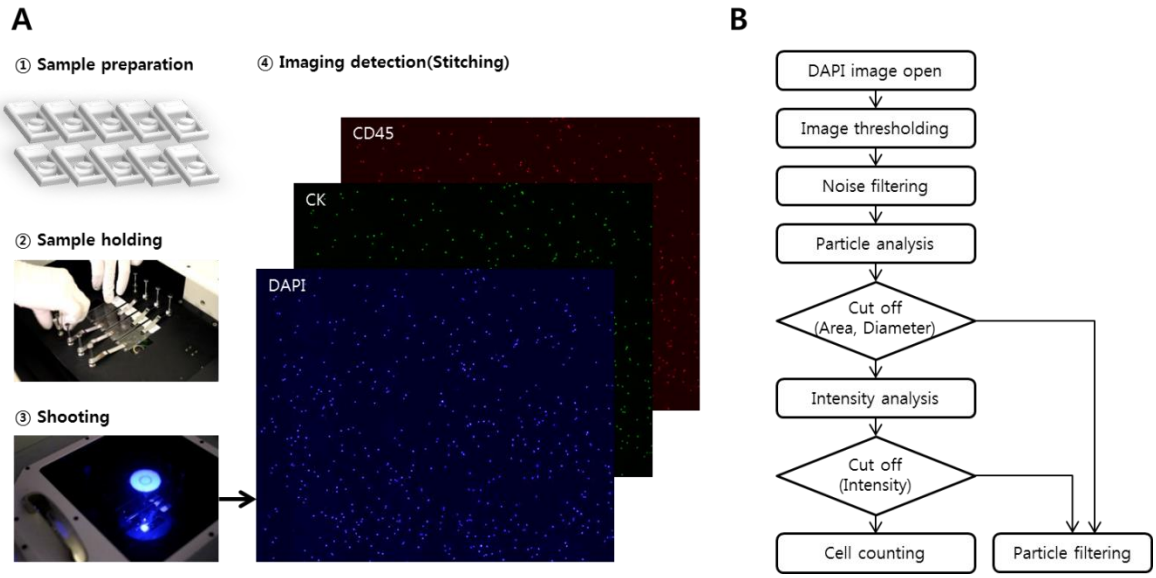
A
① Sample preparation
② Sample holding
③ Shooting
④ Imaging detection(Stitching)
CD45
CK
DAPI
B
DAPI image open
Image thresholding
Noise filtering
Particle analysis
Cut off
(Area, Diameter)
Intensity analysis
Cut off
(Intensity)
Cell counting
Particle filtering

Figure. 2

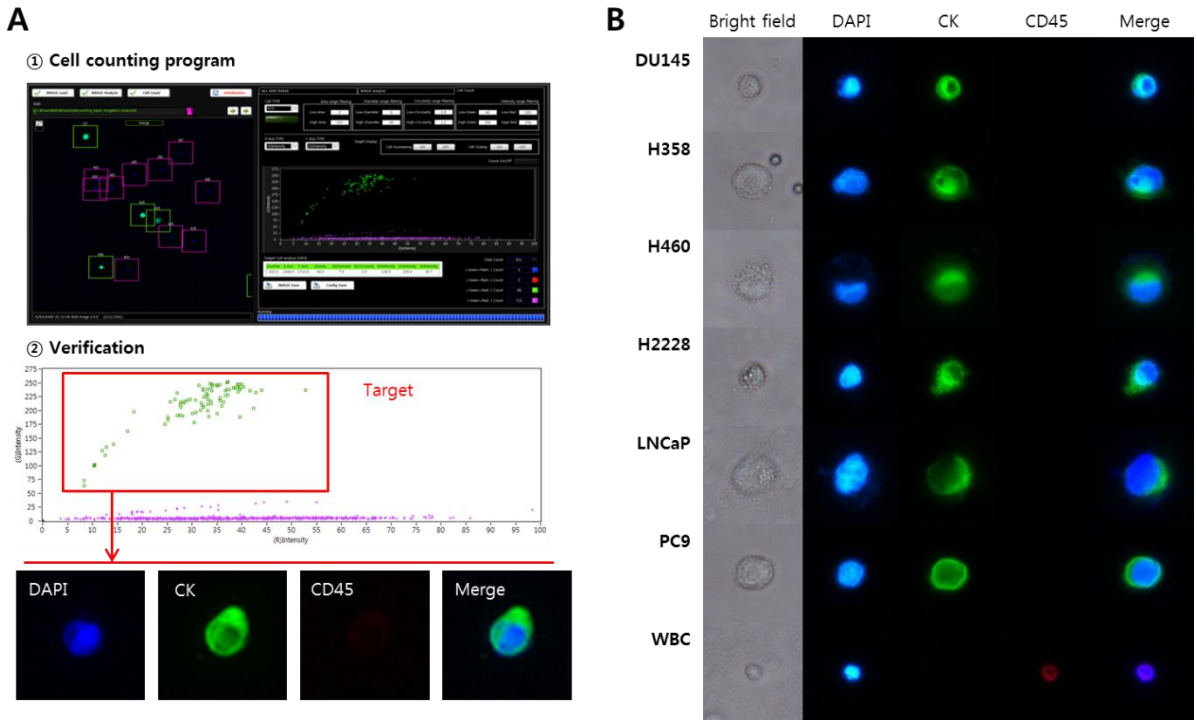
A
① Cell counting program
② Verification
Target
DAPI
CK
CD45
Merge
B
Bright field
DAPI
CK
CD45
Merge
DU145
H358
H460
H2228
LNCaP
PC9
WBC

Figure. 3

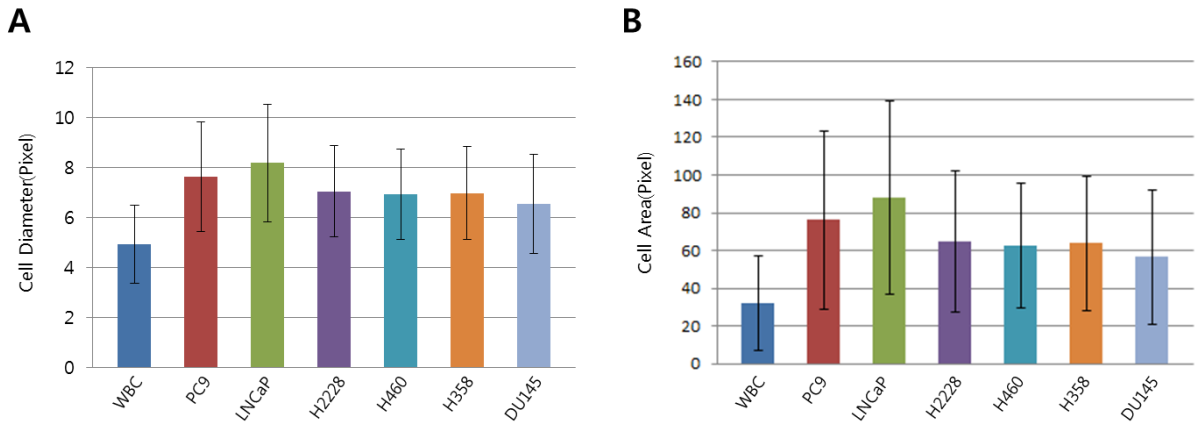
A
Cell Diameter(Pixel)
0
2
4
6
8
10
12
WBC
PC9
LNCaP
H2228
H460
H358
DU145
B
Cell Area(Pixel)
0
20
40
60
80
100
120
140
160
WBC
PC9
LNCaP
H2228
H460
H358
DU145

Figure. 4

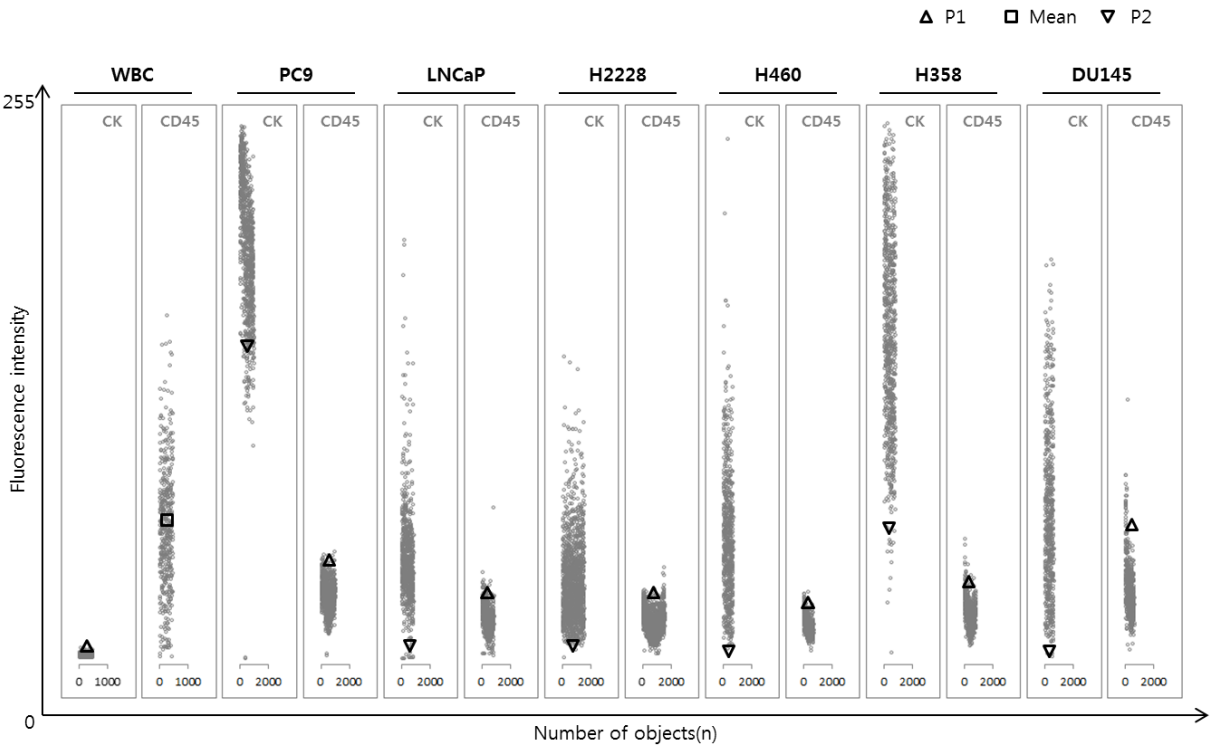
P1
Mean
P2
WBC
PC9
LNCaP
H2228
H460
H358
DU145
CK
CD45
255
0
Fluorescence intensity
Number of objects(n)
0 1000
0 2000

Figure. 5

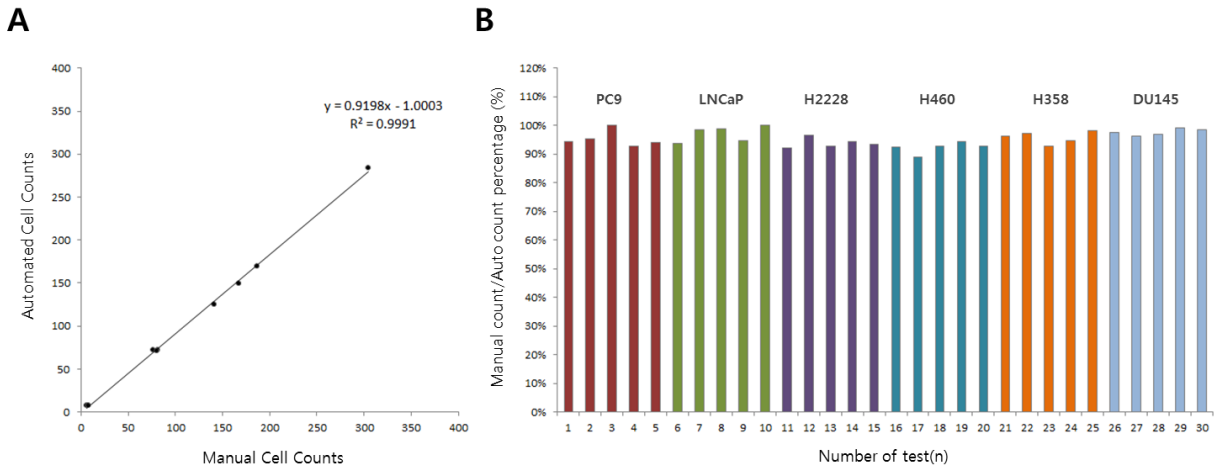
A
B
y = 0.9198x - 1.0003
R² = 0.9991
Automated Cell Counts
Manual Cell Counts
Manual count/Auto count percentage (%)
Number of test(n)
PC9
LNCaP
H2228
H460
H358
DU145